Applied Surface Science 257 (2011) 6243–6250

Contents lists available at ScienceDirect

Applied Surface Science

journal homepage: www.elsevier.com/locate/apsusc

Femtosecond laser ablation of polymeric substrates for the fabrication of microfluidic channels

Raffaella Suriano[a,*], Arseniy Kuznetsov[b], Shane M. Eaton[c], Roman Kiyan[b], Giulio Cerullo[d], Roberto Osellame[c], Boris N. Chichkov[b], Marinella Levi[a], Stefano Turri[a]

[a] Dipartimento di Chimica, Materiali e Ingegneria Chimica "Giulio Natta", Politecnico di Milano, Piazza Leonardo da Vinci 32, 20133 Milan, Italy
[b] Laser Zentrum Hannover e.V., Hollerithallee 8, 30419 Hannover, Germany
[c] Istituto di Fotonica e Nanotecnologie (IFN)-CNR, Piazza Leonardo da Vinci 32, 20133 Milan, Italy
[d] Dipartimento di Fisica, Politecnico di Milano, Piazza Leonardo da Vinci 32, 20133 Milan, Italy

ARTICLE INFO

Article history:
Received 10 October 2010
Received in revised form 11 February 2011
Accepted 13 February 2011
Available online 18 February 2011

Keywords:
Femtosecond laser
Ablation
Polymer
Microfluidics

ABSTRACT

This manuscript presents a study of physical and chemical properties of microchannels fabricated by femtosecond laser processing technology in thermoplastic polymeric materials, including poly(methyl methacrylate) (PMMA), polystyrene (PS) and cyclic olefin polymer (COP). By surface electron microscopy and optical profilometry, the dimensions of microchannels in the polymers were found to be easily tunable, with surface roughness values comparable to those obtained by standard prototyping techniques such as micromilling. Through colorimetric analysis and optical microscopy, PMMA was found to remain nearly transparent after ablation while COP and PS darkened significantly. Using infrared spectroscopy, the darkening in PS and COP was attributed to significant oxidation and dehydrogenation during laser ablation, unlike PMMA, which was found to degrade by a thermal depolymerization process. The more stable molecular structure of PMMA makes it the most viable thermoplastic polymer for femtosecond laser fabrication of microfluidic channels.

© 2011 Elsevier B.V. All rights reserved.

1. Introduction

Microfluidic devices have been the subject of extensive research in the field of analytical chemistry and biochemistry for the last two decades [1]. Polymers are rapidly emerging as the ideal substrates for such devices due to their easy processability and low cost [2]. The present work focuses on femtosecond laser ablation of polymers for the fabrication of microfluidic structures and on the study of the physicochemical modifications induced on polymer surfaces by this microfabrication technique.

To fabricate polymer microstructures at low costs and high volume, injection molding and hot embossing are the most promising techniques. Alternative fabrication techniques for prototyping are micromilling [3], UV polymerization through photomasks [4], and laser micromachining [5]. There is a growing interest in the development of these technologies with rapid prototyping capabilities because they accelerate the design and optimization of microfluidic devices. Laser micromachining is a precise, fast, clean and contactless technology suitable for prototyping of microfluidic devices in polymers [6]. When a laser is focused on the surface of a polymer substrate, material may be removed by laser ablation due to melting, evaporation and vaporization [7]. Ablation occurs above a certain threshold fluence, which depends on the material composition, wavelength, and pulse duration [8]. Ultrashort laser pulses, which concentrate energy in subpicosecond time scales, have sufficiently high peak intensity to drive nonlinear multiphoton absorption when focused on the surface of polymers, enabling laser processing at wavelengths at which the material is transparent. This is in contrast to longer pulse sources (>10 ps), where to deposit energy via linear absorption, the photon energy must be greater than the bandgap, therefore restricting the laser processing wavelength to the UV range. Another advantage of laser processing with femtosecond pulses is that since their pulse duration is shorter than the heat diffusion time, ablated features do not show heat affected zones as is the case with longer pulse sources.

Laser ablation of polymers is well known for a number of materials such as polyethylene (PE), polytetrafluoroethylene (PTFE) [9] or biodegradable polymers like polycaprolactone (PCL) and polyglycolic acid (PGA) [10]. However, the mechanism of laser ablation in polymers is complex and cannot be described by a single photochemical or mathematical model. For instance, in the case of poly(methyl methacrylate) (PMMA), up to three distinct chemical ablation mechanisms have been proposed as a function of laser parameters. Srinivasan et al. postulated a photochemical mecha-

* Corresponding author. Tel.: +39 0223994703; fax: +39 0270638173.
E-mail address: raffaella.suriano@chem.polimi.it (R. Suriano).

0169-4332/$ – see front matter © 2011 Elsevier B.V. All rights reserved.
doi:10.1016/j.apsusc.2011.02.053

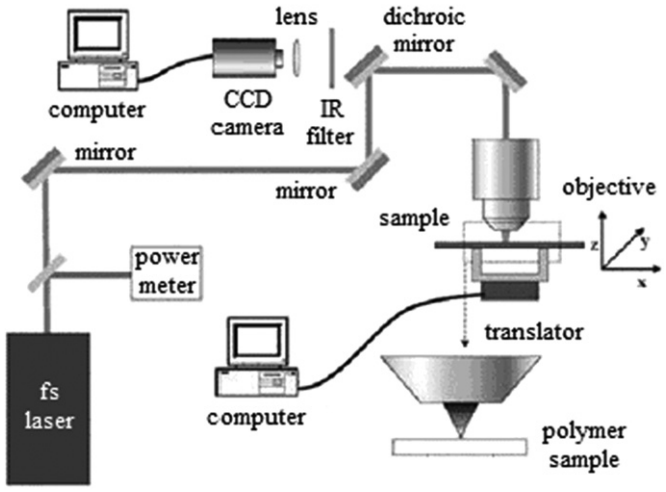

Fig. 1. Schematic of the laser micromachining setup for microchannel fabrication.

nism involving random bond breaking and short chain formation for 160 fs UV pulses [11]. A different and exclusively photothermal mechanism was described by Blanchet and Fincher for nanosecond UV pulses [12], similar to the behavior observed with continuous wave lasers [5] and to backbone cleavage by unzipping in thermal treatments [13]. Küper and Stuke found a side-chain photochemical cleavage mechanism for 300 fs UV pulses [14] and Wochnowski et al. proposed a unified mechanism using the previous results [15]. Other phenomena occurring during laser modification of polymers are incubation, i.e. the decrease of the ablation threshold with increasing number of pulses [16], and refractive index changes at sub-ablation laser fluences, which can be exploited for waveguide writing [17].

Relatively little work has so far been performed on femtosecond laser ablation of polymer substrates for microfluidics, focused mainly on polydimethylsiloxane (PDMS) and PMMA substrates [18,19]. In this work, we perform a comprehensive study of the properties of femtosecond laser-ablated polymer surfaces in view of microfluidic channel fabrication. We studied several thermoplastic polymers commonly used for microfluidics, namely PMMA, cyclic olefin polymer (COP), and polystyrene (PS). We apply different characterization techniques including infrared spectroscopy, electron microscopy and optical profilometry to study the degradation mechanisms and the surface properties following laser ablation.

2. Materials and methods

2.1. Materials

All raw polymer samples (PMMA, PS and COP) were supplied by Microfluidic ChipShop GmbH (Jena, Germany); they consist of injection-molded plates (75.5 mm × 25.5 mm) which were used as substrates for the laser ablation experiments.

2.2. Femtosecond laser processing and microchannel fabrication

The setup used for the fabrication of microchannels is shown in Fig. 1. It consists of a regeneratively amplified Ti:Sapphire femtosecond laser system (Spectra-Physics Spitfire Pro XP). The main parameters of this laser system are listed in Table 1. The output laser beam is directed towards the focusing objective by 100% reflecting mirrors. For micromachining of polymer materials, the laser beam is focused onto the material surface by a lens with 125 mm focal distance. The focal spot diameter, d is equal to 16 μm and was

Table 1
Characteristics of the Spectra-Physics Spitfire Pro XP Ti:Sapphire regenerative amplifier system.

Wavelength	800 nm
Maximum average output power	3.5 W
Maximum pulse energy	3.5 mJ
Repetition rate	1 kHz
Pulse duration	40 fs
Output beam diameter	~8 mm

estimated according to the following equation:

$$d = \frac{4\lambda f}{\pi D} \quad (1)$$

where λ is the laser beam wavelength, f is the focal length of the lens and D is the laser beam diameter before final focusing lens. We also observed that this estimated value is very similar to the width of single scan microchannels obtained with laser power close to the ablation threshold.

Laser power is adjusted by a step attenuator with fixed attenuation, with a combination of λ/2-waveplate and a polarizing beam splitter offering finer control and used in the computer controlled feedback loop to compensate for drift of the output laser power and provide constant and reproducible structuring conditions over long time intervals. The sample is positioned with respect to the focused laser beam by a computer controlled linear translation system. Two translation stages (Physik Instrumente M-511.DD) for x and y axes, and one stage (Physik Instrumente M451.DG) for the z-axis with micrometer resolution and travel ranges of 100 mm × 100 mm × 12.5 mm were used for the experiments. Microfluidic channels of similar dimensions as those fabricated by femtosecond laser ablation were produced by Institut für Mikrotechnik Mainz GmbH (Mainz, Germany) with a micromilling machine (Charlyrobot SAS) and used for benchmarking the surface roughness results.

2.3. Environmental scanning electron microscopy (ESEM)

The scanning electron microscope used in this work is an EVO 50® extended pressure instrument (ZEISS). This microscope works in a continuous vacuum up to 3000 Pa, and allows the differentiation of the vacuum degree between the filament chamber and the sample-holder chamber due to a valve system. The electron source is a LaB_6 nanocrystal. Electrons are accelerated by a potential difference of 20 kV, and the primary beam has an intensity of 250 pA. The shape of microchannels obtained was determined by ESEM after cryo-fracturing them in liquid nitrogen. Samples were dipped in liquid nitrogen for 10 min, in order to exploit cold embrittlement of polymers. The direction of the fracture was always perpendicular to the channels.

2.4. Profilometry

Surface roughness was measured according to DIN 4768 [20] using a laser profilometer (UBM Microfocus) with a maximum vertical resolution of 6 nm and a maximum vertical range of ±500 μm. In the horizontal direction, the profilometer measures 1400 points/mm, giving a point separation (resolution) Δx_{pr} of roughly 0.7 μm per point. For each 2-D profile, a 1.75 mm length was measured along the x-axis, with only the central portion of 1.25 mm evaluated. The following topographic parameters were measured:

- R_a, the arithmetic average of the absolute value of all the profile points

$$R_a = \frac{1}{N}\sum_{n-1}^{N}|Z_i| \quad (2)$$

where z_i is the vertical distance from the mean line to the ith data point and N is the number of points in the analyzed profile.
- R_q, root mean square roughness, which is the root mean square average of measured values of the roughness profile,
- R_t, the maximum peak-to-valley height of the entire measurement trace.

2.5. Colorimetric analysis

Colorimetric measurements were performed with a spectrophotometer (Konica Minolta CM-2600d), which allows an accurate analysis of the macroscopic color features of the surface. The measurement area is circular with a diameter of about 10 mm, enabling the simultaneous measurement of several ablated channels. Measurements were expressed by coordinates L^*, a^*, b^* in the CIEL$^*a^*b^*$ color space [21]. The CIEL$^*a^*b^*$ colorimetric system defines the colors by three numerical values. L^* is the lightness intensity of the color on a scale ranging from 0 (black) to 100 (white). The positive a^* value indicates the red color while the negative a^* value represents the green color. Similarly, positive and negative b^* values indicate the yellow and the blue colors, respectively. Results are expressed as the difference in coordinates ΔL^*, Δa^*, Δb^* between standard and treated (laser ablated) samples.

2.6. Attenuated total reflectance-Fourier transform infrared spectrometer (ATR-FTIR)

Vibrational spectra inside and outside the channels were acquired using an FTIR spectrometer in ATR mode (Perkin Elmer Spectrum 2000), equipped with a Si microcrystal tip having a contact diameter of 100 μm. The small tip dimensions allowed the measurements of IR spectra also inside the channels. Spectra were collected (64 scans, resolution 4 cm^{-1}) in the wavenumber range of 700–4000 cm^{-1}. Each measurement was performed after the acquisition of the spectrum of the surrounding air as a background.

2.7. Gel permeation chromatography (GPC)

Molecular weight measurements on solvent extracted samples have been performed using a Waters 510 GPC apparatus working in tetrahydrofurane (THF) at 40 °C, equipped with a set of Ultrastyragel® columns and a Waters 410 differential diffractometer as detector. Two different calibrations have been employed, the former with different monodisperse fractions of PS, and the latter with PMMA fractions. For GPC analysis, the material on the bottom of the microchannels was carefully etched and removed with fresh THF droplets using a syringe. About 10–12 mg of material from the channels was extracted and analyzed by GPC.

3. Results and discussions

3.1. Laser processing

Surface microchannels were fabricated in PMMA, PS and COP substrates by single-scan and multi-scan laser ablation. Single-scan microchannels were fabricated at various scan speeds, ranging from 100 μm/s to 5 mm/s, while the laser beam fluence (average power) was varied over three values, namely 8.8 J/cm^2 (10 mW), 44.2 J/cm^2 (50 mW) and 88.4 J/cm^2 (100 mW). Single-scan channels typically have "V" or "U" shape depending on the polymer characteristics. The width and depth of the channels is defined by polymer type, geometrical characteristics of the focused laser beam, average laser power, and structuring speed. The depths of the fabricated microchannels are reported in the subsequent Section 3.2.

To form microchannels with easily tailored depth and width, a multi-scan technique was applied, where the sample was shifted horizontally and orthogonally to the scan direction between scans. The best compromise between processing speed and smooth channel floors was obtained with 6 μm distance between the adjacent horizontal scans. Several sets of channels were fabricated by the multi-scan technique in all polymers by variation of the laser fluence and scan speed in the same ranges explored for the single scan production.

ESEM analysis of the microchannels fabricated by the multi-scan technique (discussed in details in the next section) allowed to estimate the amount of ablated material and thus provided the characterization of the removal rate as a function of the processing parameters (see Fig. 2). It can be noticed that the removal rate with femtosecond laser processing is in the order of 1–4 × 10^6 μm^3/s, which is a few orders of magnitude lower than that achievable by micromilling; however, as will be seen in the next sections, femtosecond laser processing provides a much greater control on the amount of removed material, does not suffer from any tool wear and creates smoother channels. Further, recently available amplified femtosecond laser systems operating at ~1 MHz repetition rate could bridge the gap with micromilling in terms of processing efficiency.

Fig. 2 shows that the removal rate strongly depends on the laser fluence, yielding a significant rate increase; however, at low scan speeds, the surface of some polymers was severely damaged by high fluence femtosecond laser pulses. Corresponding points are not shown in the graphs. PMMA and PS provide a slightly higher removal rate compared to COP. This can be explained by a lower wavelength absorption edge of COP, thus resulting in a more nonlinear absorption process with a reduced efficiency [22].

On the other hand, the dependence of the removal rate on the processing speed shows a clear saturation, thus indicating that at speeds higher than 1 mm/s the faster processing is compensated by a lower amount of material removed. Notwithstanding the equivalent removal rate, the surface quality achieved at 1 mm/s and 5 mm/s is significantly different, as shown in Fig. 3, with a superior uniformity at 5 mm/s. For this reason all the experimental results presented in the following sections have been achieved at a processing speed of 5 mm/s.

3.2. Morphological and surface characterization

Single scan laser ablation experiments produced narrow, strongly V-shaped channels, similar to those reported in the literature [5,23]. The shape of ablated microchannels can be visualized by ESEM after cryo-fracturing in liquid nitrogen. Typical channel profiles from single scans in PMMA and PS are shown in Fig. 4.

As shown in Fig. 4, the cross-section profile of PS (b) is sharper and deeper than that of PMMA (a). Since all the polymeric samples were ablated with the same processing parameters, the differences in channels shape and geometry should involve a different response by the polymer substrate, related to its absorption edge wavelength, molecular weight, T_g or to the laser ablation mechanism. As far as final application is concerned, microchannels should preferably have a circular or rectangular shape for ideal flow through microfluidic channels [24]. Consequently, the aforementioned multi-scan ablation geometry was applied. ESEM images of multi-scan microchannels are shown in Fig. 5 for PMMA, PS and COP.

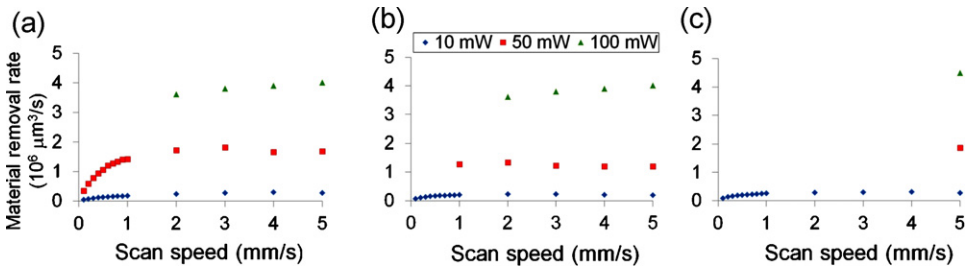

Fig. 2. Material removal rate versus scan speed for (a) PMMA, (b) COP and (c) PS for powers of 10, 50 and 100 mW. Error values are due to surface roughness of channels. Maximum percentage error of 7.6% (error bars too small to be shown on graph) occurs for lowest fluence and maximum speed, where the shallowest channels were obtained.

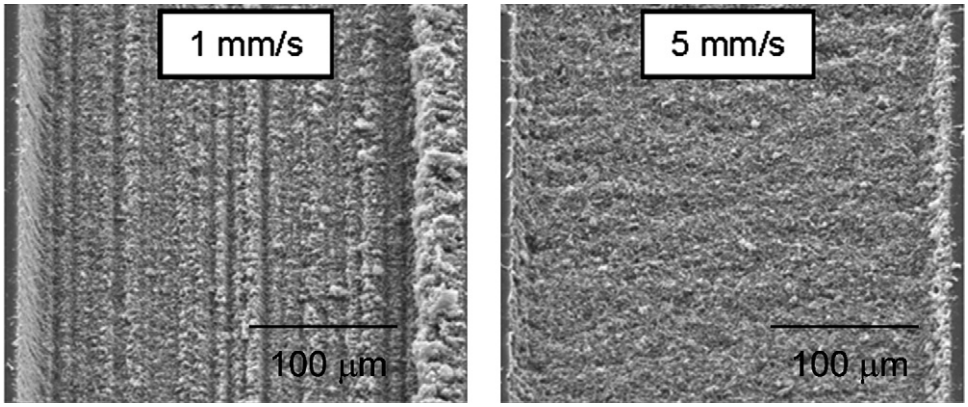

Fig. 3. ESEM images of the ablated microchannels in PMMA substrates. The average laser power is 10 mW; scan speeds are 1 mm/s and 5 mm/s.

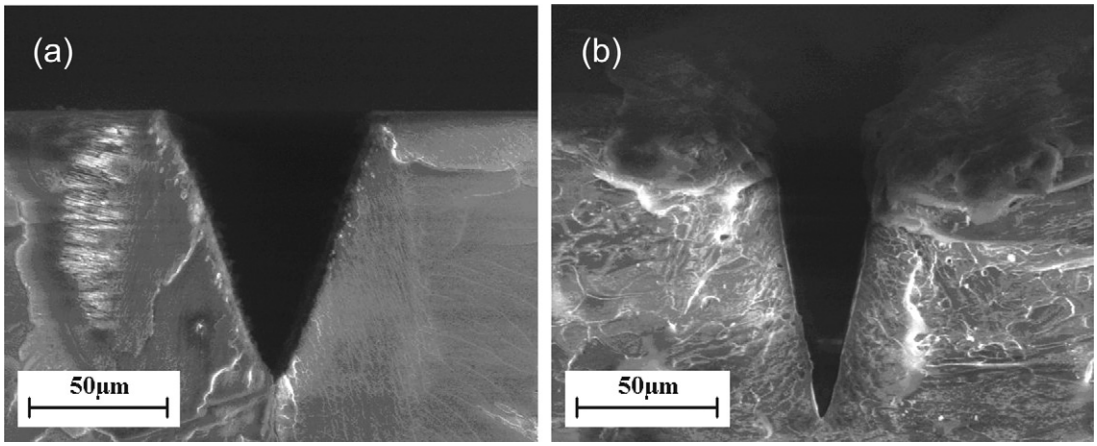

Fig. 4. ESEM images of single-scan microchannels for PMMA (a) and PS (b).

Profile contours show some debris and burrs at the edges: they could be either a product of the cold fracture or small bumps of resolidified material produced during the ablation process. Evidence of resolidified molten materials was also previously observed on ablation contours of PMMA and polycarbonate obtained by IR-femtosecond laser ablation [16].

Shallow and wide channels were easily obtained, suitable for the subsequent characterization steps. The cross-sections of channels obtained with femtosecond laser using the multi-scan technique are nearly trapezoidal in all cases. The channel depth is material dependent also in multi-scan mode (Fig. 6): channels in PS and PMMA are deeper compared to those in COP. This confirms the less efficient ablation in COP due to its higher bandgap compared to PMMA and PS [22]. As expected, the ablation depth increases with laser fluence for each polymer.

For laser fluences applied in our experiments the ablation depth increases with laser fluence for each polymer as previously observed in literature [25].

Some darkening due to ablation is evident for PS and COP samples, whereas the PMMA channels remained optically transparent for all the fluence values employed. The ablated areas inside COP and PS channels become darkened when ablated with high fluences. In the case of PS microchannels obtained with 44.2 J/cm^2, a layer of very dark material on the bottom surface of the channel is visible even by naked eye. Heat affected zones are also evident in Fig. 5(b) for PS samples as darkened regions on the left below the bottom surface of microchannel. It may be an indication of severe oxidative degradation involved in the chemical mechanism of femtosecond laser ablation of the material.

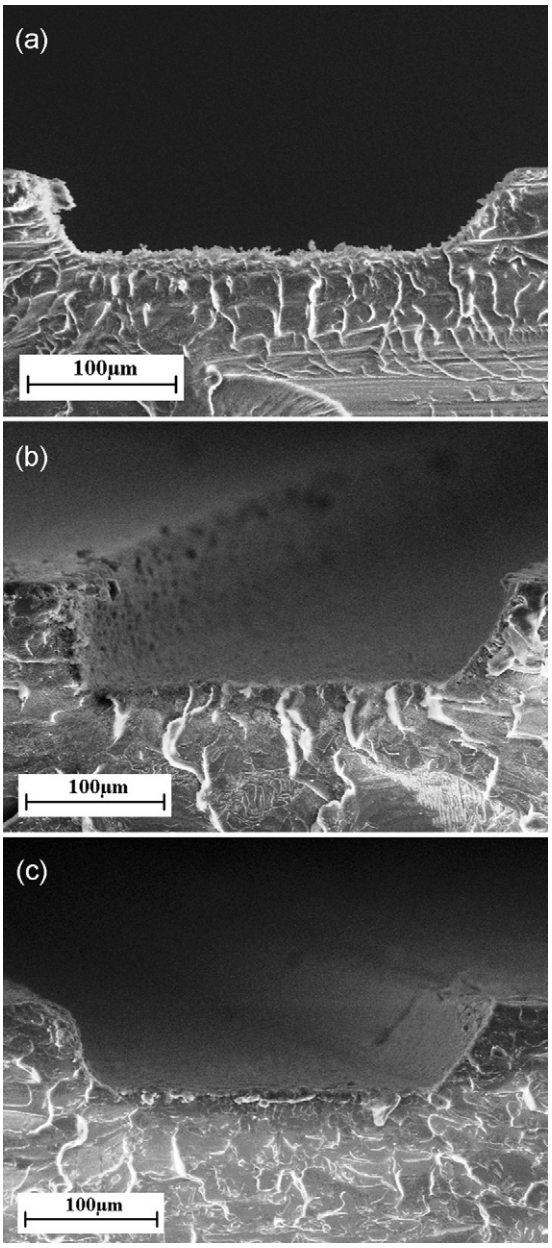

Fig. 5. Multi-scan microchannels ablated at 44.2 J/cm^2 in PMMA (a), in PS (b) and in COP (c).

To give a semi-quantitative measurement of sample darkening, a colorimetric analysis was performed as explained in the experimental section. Fig. 7 exhibits ΔL^* changes as a function of laser fluence for all the ablated surfaces: it confirms the significant darkening particularly of PS ablated at higher fluence. A linear decrease of lightness also appears for COP by increasing processing fluence, whereas lightness of PMMA samples is only slightly affected by laser ablation. Yellowing is quantified by Δb^* values: the effect is noteworthy only for PS and COP ablated with 44.2 and 88.4 J/cm^2 (data not shown), whereas there was no considerable change for the parameter a^* for all the investigated materials.

Linear profilometry was performed on pristine injection molded samples and on the bottom surface of laser-ablated microchannels. The longitudinal direction of the microchannels was always chosen as the direction for the profilometer scans. The results are summarized in Table 2. Laser ablation increases significantly the average surface roughness of the polymers. In particular, PS chan-

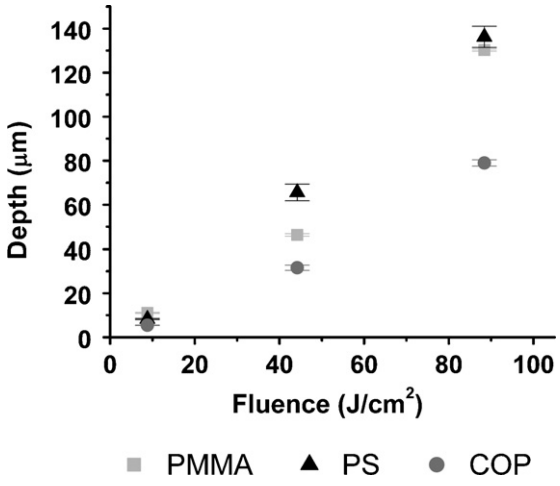

Fig. 6. Microchannels depth vs. processing fluence values for all the substrates employed. Measurements are presented as averages ± the standard deviation, which is represented as error bars.

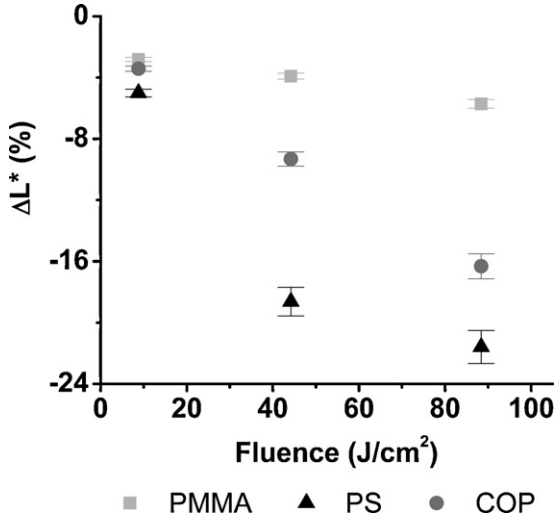

Fig. 7. Variation of lightness (ΔL^*) as a function of laser fluence for the ablated samples in comparison with bare substrates ($\Delta L^* = L^*_{\text{abl. sample}} - L^*_{\text{bare}}$). Measurements are presented as averages ± the standard deviation, which is represented as error bars.

Table 2
Longitudinal roughness parameters (average roughness, R_a, root mean square roughness, R_q, the maximum peak-to-valley height, R_t, averages ± standard deviation (SD)) of untreated injection molded samples and microchannels ablated with different laser fluences and micromilled.

	Fluence (J/cm^2)	$R_a \pm$ SD (μm)	$R_q \pm$ SD (μm)	$R_t \pm$ SD (μm)
PMMA				
Untreated	0	0.026 ± 0.010	0.035 ± 0.009	0.317 ± 0.063
	8.8	0.235 ± 0.066	0.296 ± 0.091	1.675 ± 0.486
Ablated	44.2	0.284 ± 0.040	0.354 ± 0.043	1.962 ± 0.250
	88.4	0.345 ± 0.052	0.453 ± 0.074	2.758 ± 0.541
Micromilled	–	0.164 ± 0.021	0.213 ± 0.034	1.307 ± 0.171
PS				
Untreated	0	0.036 ± 0.025	0.065 ± 0.045	0.756 ± 0.583
	8.8	0.338 ± 0.070	0.411 ± 0.085	2.001 ± 0.313
Ablated	44.2	0.312 ± 0.167	0.396 ± 0.217	2.301 ± 1.274
	88.4	0.561 ± 0.084	0.700 ± 0.109	3.497 ± 0.455
Micromilled	–	0.328 ± 0.040	0.416 ± 0.049	2.550 ± 0.418
COP				
Untreated	0	0.035 ± 0.003	0.050 ± 0.012	0.498 ± 0.309
	8.8	0.123 ± 0.055	0.153 ± 0.069	0.919 ± 0.419
Ablated	44.2	0.148 ± 0.032	0.178 ± 0.051	1.107 ± 0.297
	88.4	0.186 ± 0.088	0.238 ± 0.119	1.431 ± 0.736
Micromilled	–	0.224 ± 0.124	0.275 ± 0.151	1.562 ± 0.634

nels are noticeably rougher. Femtosecond laser ablation produces microchannels with surface quality comparable with that achieved by micromilling, but with the added advantage of enabling on-the-fly adjustments in the microchannel geometry. Further, laser processing does not suffer from toolwear as the direct contact micromilling technique.

3.3. Chemical surface modifications and degradation

The vibrational spectra were recorded for pristine polymer as well as for all laser-ablated microchannels with an ATR probe, which has a sampling depth of around 1–2 μm. This technique is able to characterize the material in the vicinity of the ablated surface. The ATR infrared spectra of PMMA before and after femtosecond laser ablation were overlapped for comparison and attention was especially given to the stretching region of C—H bonds (2800–2900 cm^{-1}) and C=O bonds (1700–1800 cm^{-1}). Details of spectra are shown in Fig. 8. These bands were chosen for monitoring possible degradation phenomena, since any oxidation process of the polymer would involve a decrease in C—H intensity and a corresponding increase in C=O stretching band.

No evident differences exist before and after laser ablation of PMMA. The ratio between absorbance intensities of peaks belonging to C=O and to C—H stretching for each spectrum gives the carbonyl index, calculated according to the following equation [26]:

$$\text{Carbonyl Index} = \frac{\max A_{C=O}\ \text{str}}{\max A_{C-H}\ \text{str}} \quad (3)$$

This parameter was found to remain nearly constant with increasing laser fluence: the index is 7.01 ± 2.27 and 6.17 ± 1.33 for 0 and 88.4 J/cm^2 fluence, respectively. These results suggest that functional groups of PMMA do not change significantly after laser ablation. The lack of an evident oxidation process was already reported for PMMA samples ablated by femtosecond laser and confirmed by X-rays Photoelectron and FTIR spectroscopy in our previous work [25].

Spectra of ablated and untreated PS and COP are shown in Figs. 9 and 10, respectively. After laser ablation these polymers show some changes in their IR spectra, namely the appearance of absorptions due to —OH groups (3400–3600 cm^{-1}) and of broad bands attributed to carbonylic species at around 1700 cm^{-1}. For COP, at least two different oxidized species are formed, with a corresponding reduction of C—H signals intensity. A band related to C=C stretching can be seen in laser-ablated COP near 1620 cm^{-1}, but it is not well resolved being a shoulder of the carbonyl band.

3.3.1. GPC

A further investigation of molecular changes induced by laser processing was done through molecular weight measurements. This was carried out by carefully etching the surface of ablated microchannels with solvent (THF), and analyzing the extracted polymer by GPC. In such case the measurement samples the first polymer layers close to the ablated area and therefore includes unmodified macromolecules of the bulk material close to the surface. The main results are shown in Table 3.

There was a slight decrease in the molecular weight for PMMA, while no comparison can be made for COP since the pristine polymer was not completely soluble in THF. It is interesting to observe that the laser-ablated zones of PS are very dark, and these parts could not be dissolved in THF; this behavior is consistent with the

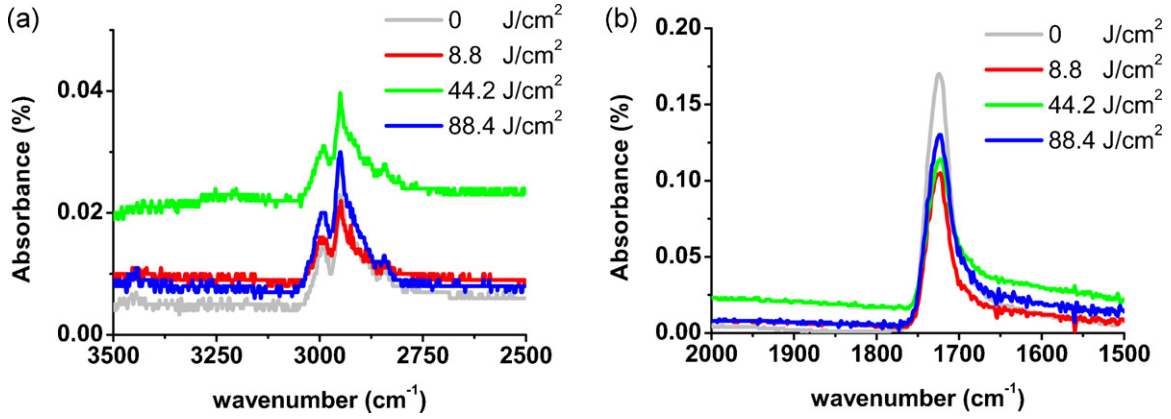

Fig. 8. Details of μ-ATR-FTIR spectra corresponding to the absorptions of C—H stretching (a) and C=O stretching (b) for untreated and laser-ablated PMMA samples.

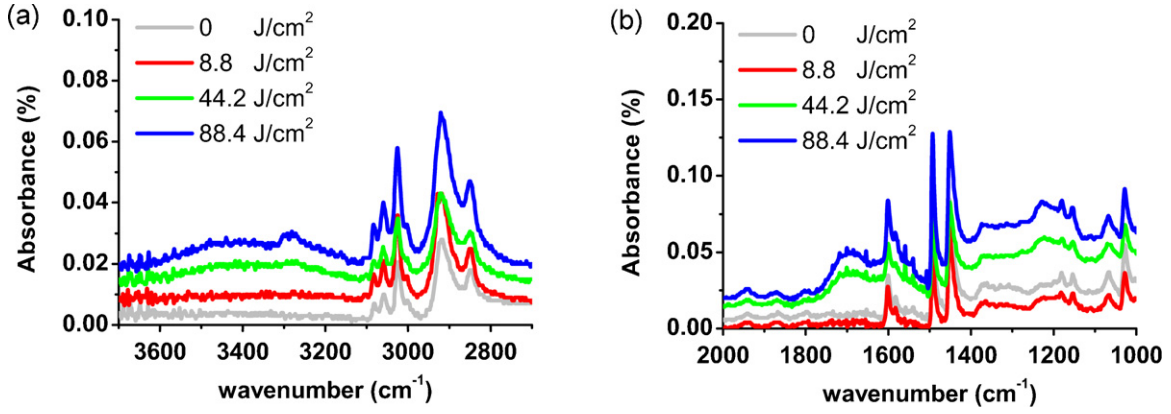

Fig. 9. Details of μ-ATR-FTIR spectra for untreated and laser-ablated PS samples: wavelength range from 3700 to 2700 cm^{-1} (a) and from 2000 to 1000 cm^{-1} (b).

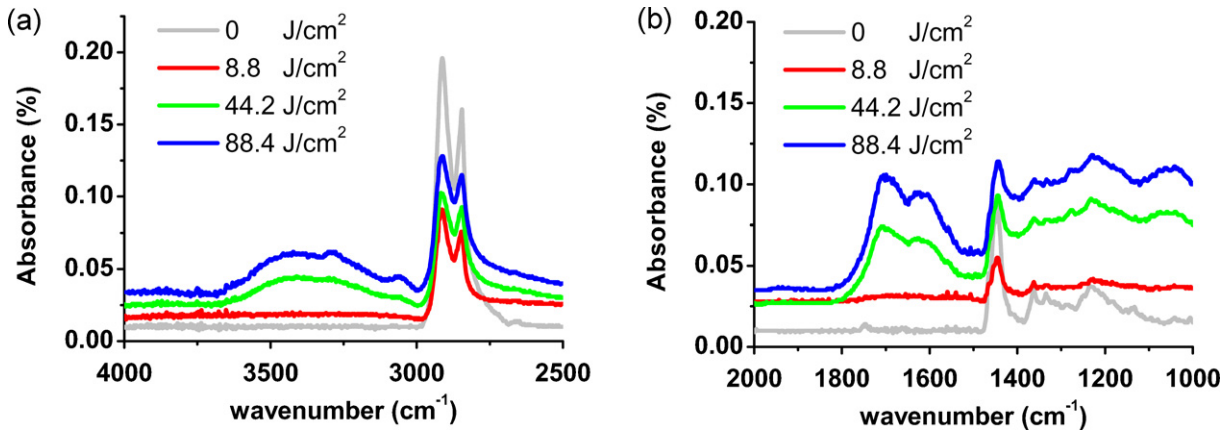

Fig. 10. Details of μ-ATR-FTIR spectra for untreated and laser-ablated COP samples: wavelength range from 3700 to 2700 cm^{-1} (a) and from 2000 to 1000 cm^{-1} (b).

Table 3
Molecular weight measurements by GPC for untreated substrates and for microchannels ablated at 44.2 J/cm^2.

Sample		M_n	M_w	M_p	Polidispersity index
PMMA	Untreated	75000	117900	130650	1.57
	Treated	54000	109100	126800	2.02
PS	Untreated	156000	32700	322200	2.10
	Treated	200100	329050	320450	1.64
COP	Untreated	n/a	n/a	n/a	n/a
	Treated	171000	351200	266200	2.05

formation of a heavily crosslinked conjugated polymer surface or carbonaceous structures.

3.3.2. Degradation mechanism of PMMA

In PMMA, the analytical results can be briefly summarized as follows. Femtosecond laser ablation at the wavelength of 800 nm produces nearly uncolored structures in PMMA. The chemical functional groups of the polymer remain unaffected. Its molecular weight decreases with ablation. PMMA is completely soluble in THF before and after laser ablation. These results suggest a thermal degradation mechanism in PMMA [27]. This mechanism is a process inverse to polymerization, in which the polymer reverts to monomer, called unzipping [28]. As seen in the vibrational spectra, no new evident functional groups appear. Unzipping may justify the average molecular weight reduction since monomer passes to gas phase decreasing the polymer chain length.

This mechanism is in disagreement with some literature reports on PMMA laser ablation. Chemical modification of the structure has been largely found, and mechanisms involving side chain cleavage have been proposed for femtosecond laser ablation of PMMA [14,15]. It is however important to underline that these studies on PMMA ablation have mainly focused on the use of UV laser pulses, which deliver more energetic photons compared to the near-IR Ti:Sapphire laser sources employed in this work.

3.3.3. Degradation mechanism of PS

Excimer laser ablation of PS has been reported to be a photothermal process [29]. The non-oxidative unzipping mechanism is also possible for PS according to classical literature data, however a quantitative reversion to monomer cannot occur since other degradation pathways are always present [28]. A general hydroperoxidation of benzylic hydrogen can also occur generating oxy-macroradicals. The oxy-macroradicals may evolve to aryl-ketones, aryl-aldehydes, and tertiary as well as secondary alcohols

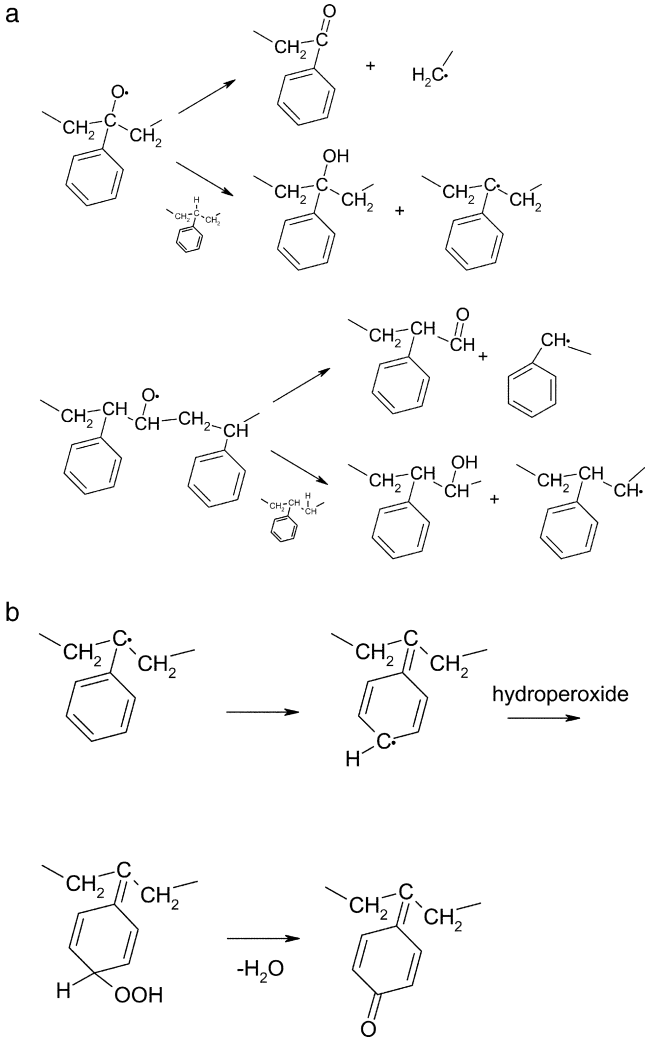

Fig. 11. Scheme of the mechanism of PS photothermal degradation: (a) formation of aryl-ketones, aryl-aldehydes, and secondary and tertiary alcohols, (b) formation of quinonoid structures.

depending on the position of H-abstraction as shown in the scheme in Fig. 11(a) [30].

The IR absorption bands of such species are consistent with the spectra reported before (Fig. 9(b)). The aryl aldehydic groups are in fact known to absorb in the band 1695–1715 cm^{-1} and the absorption bands of aryl ketonic groups are near 1680–1700 cm^{-1}.

Termination of the macroradicals in PS chains by disproportionation can form C=C double bonds, which can produce branching [31] and eventually lead to crosslinking [32]. Moreover, unsaturated end groups can be generated by β-scission reactions. Such reactions can also produce α-ω dialkenes from macroradicals of heavier alkenes [33]. All these degradation pathways could justify the formation of very dark, insoluble compounds on PS laser-ablated samples.

The development of the highly colored products can be attributed to the double bond shift in the initially formed PS radical, leading to a quinonoid structure after dehydration of a hydroperoxide, as shown in Fig. 11(b) [28]. The presence of quinonoid structure is consistent with IR absorption belonging to C=O stretching of quinone (1655–1690 cm^{-1}), detected inside the microchannels formed at higher laser fluence (at 44.2 and 88.4 J/cm^2, see Fig. 9(b)).

3.3.4. Degradation mechanism of COP

Polymer oxidation is evident by the complex IR absorptions in the range of 1650–1750 cm^{-1}. The peak at ~1710 cm^{-1} is likely due to C=O stretching, while the shoulder at 1610–1645 cm^{-1} is attributed to C=C stretching. A mechanism of dehydrogenation is consistent with the decrease in aliphatic C—H vibrations (2800–2950 cm^{-1}), and with the appearance of a low intensity C=C—H stretching band just above 3000 cm^{-1}. Moreover, the surface of this polymer has shown to turn to yellow-brown after laser ablation. This suggests the formation of some visible light-absorbing functional groups, such as conjugated double C=C bonds. Results from GPC analysis indicate the occurrence of degradation phenomena (improved solubility due to molecular weight and/or polarity changes), but not their nature. The degradation route can be a combination of oxidation and dehydrogenation. This is consistent with the degradation mechanism already reported in literature for some cyclic olefin copolymers [34].

4. Conclusions

Many analytical techniques have been employed in this work to assess the effect of femtosecond laser pulses on the morphological features and changes in chemical structure of thermoplastic polymers commonly used in microfluidics. Laser processing parameters were adjusted to obtain controlled morphology microchannels with tunable widths and depths. The average surface roughness of ablated areas is lower than 400 nm, comparable to that achieved by a standard mechanical method such as micromilling, with the advantage of a higher flexibility in patterning.

The main mechanisms of polymer modification and degradation caused by laser pulses have been investigated. PMMA was found to be the most stable polymer structure with respect to laser processing. In particular, we attribute PMMA degradation to a thermal depolymerization/unzipping process, whereas both COP and PS are found to undergo extensive oxidation and dehydrogenation during laser ablation.

Acknowledgements

This work was supported by the European Commission, FP7 Project Contract no. ICT-2007-224205 (microFLUID – micro-Fabrication of polymeric Lab-on-a-chip by Ultrafast lasers with Integrated optical Detection). The authors thank the Institut für Mikrotechnik Mainz (IMM), Germany, for providing micromilled samples and Dario Picenoni for ESEM images.

References

[1] D.R. Reyes, D. Iossifidis, P.A. Auroux, A. Manz, Micro total analysis systems. 1. Introduction, theory, and technology, Anal. Chem. 74 (2002) 2623–2636.
[2] H. Becker, L.E. Locascio, Polymer microfluidic devices, Talanta 56 (2002) 267–287.
[3] P. Rai-Choudhury, Handbook of Microlithography, Micromachining, and Microfabrication, vol. 2: Micromachining and Microfabrication, SPIE-International Society for Optical Engineering Press, Wellingham, Washington, USA, 1997, 338–345.
[4] S. Turri, M. Levi, E. Emilitri, R. Suriano, R. Bongiovanni, Direct photopolymerisation of PEG-methacrylate oligomers for an easy prototyping of microfluidic structures, Macromol. Chem. Phys. 211 (2010) 879–887.
[5] H. Klank, J.P. Kutter, O. Geschke, CO_2-laser micromachining and back-end processing for rapid production of PMMA-based microfluidic systems, Lab Chip 2 (2002) 242–246.
[6] B.N. Chichkov, C. Momma, S. Nolte, F. von Alvensleben, A. Tunnermann, Femtosecond, picosecond and nanosecond laser ablation of solids, Appl. Phys. A: Mater. Sci. Process. 63 (1996) 109–115.
[7] R. Srinivasan, W.J. Leigh, Ablative photodecomposition: action of far-ultraviolet (193 nm) laser radiation on poly(ethylene terephthalate) films, J. Am. Chem. Soc. 104 (1982) 6784–6785.
[8] C. Khan Malek, Laser processing for bio-microfluidics applications (part I), Anal. Bioanal. Chem. 385 (2006) 1351–1361.
[9] J. Kruger, W. Kautek, Femtosecond-pulse visible laser processing of transparent materials, Appl. Surf. Sci. 96–8 (1996) 430–438.
[10] C.A. Aguilar, Y. Lu, S. Mao, S.C. Chen, Direct micro-patterning of biodegradable polymers using ultraviolet and femtosecond lasers, Biomaterials 26 (2005) 7642–7649.
[11] R. Srinivasan, B. Braren, R.W. Dreyfus, L. Hadel, D.E. Seeger, Mechanism of the ultraviolet-laser ablation of poly(methyl methacrylate at 193 and 248 nm – laser-induced fluorescence analysis, chemical-analysis, and doping studies, J. Opt. Soc. Am. B-Opt. Phys. 3 (1986) 785–791.
[12] G.B. Blanchet, C.R. Fincher Jr., Laser induced unzipping: a thermal route to polymer ablation, Appl. Phys. Lett. 65 (1994) 1311–1313.
[13] I. Mita, Effect of structure on degradation and stability of polymers, in: H.H.G. Jellinek (Ed.), Aspects of Degradation and Stabilization of Polymers, Elsevier, Amsterdam, 1996, pp. 247–294.
[14] S. Küper, M. Stuke, Femtosecond uv excimer laser ablation, Appl. Phys. B: Photophys. Laser Chem. 44 (1987) 199–204.
[15] C. Wochnowski, S. Metev, G. Sepold, UV-laser-assisted modification of the optical properties of polymethylmethacrylate, Appl. Surf. Sci. 154–155 (2000) 706–711.
[16] S. Baudach, J. Bonse, J. Kruger, W. Kautek, Ultrashort pulse laser ablation of polycarbonate and polymethylmethacrylate, Appl. Surf. Sci. 154 (2000) 555–560.
[17] A. Baum, P.J. Scully, M. Basanta, C.L.P. Thomas, P.R. Fielden, N.J. Goddard, W. Perrie, P.R. Chalker, Photochemistry of refractive index structures in poly(methyl methacrylate) by femtosecond laser irradiation, Opt. Lett. 32 (2007) 190–192.
[18] D. Gomez, F. Tekniker, I. Goenaga, I. Lizuain, M. Ozaita, Femtosecond laser ablation for microfluidics, Opt. Eng. 44 (2005) 051105.
[19] D.B. Wolfe, J.B. Ashcom, J.C. Hwang, C.B. Schaffer, E. Mazur, G.M. Whitesides, Customization of poly(dimethylsiloxane) stamps by micromachining using a femtosecond-pulsed laser, Adv. Mater. 15 (2003) 62–65.
[20] Rule «DIN 4768» Deutsches Institut für Normung, 1990.
[21] Commission Internationale de l'Eclairage, Publication 15: 2004, Colorimetry, Vienna: CIE Central Bureau, 2004.
[22] F. Träger (Ed.), Springer Handbook of Lasers and Optics, Springer, New York, 2007, p. 319.
[23] J.Y. Cheng, C.W. Wei, K.H. Hsu, T.H. Young, Direct-write laser micromachining and universal surface modification of PMMA for device development, Sens. Actuators B 99 (2004) 186–196.
[24] H. Bruus, Theoretical Microfluidics, Oxford University Press, New York, 2008.
[25] C. De Marco, S.M. Eaton, R. Suriano, S. Turri, M. Levi, R. Ramponi, G. Cerullo, R. Osellame, Surface properties of femtosecond laser ablated PMMA, ACS Appl. Mater. Interfaces 2 (2010) 2377–2384.
[26] A. Hogt, Modification of polypropylene with maleic anhydride, in: ANTEC '88 Proceedings of the 46th Annual Technical Conference, 18–21 April, Atlanta, 1988, pp. 1478–1480.
[27] H.H.G. Jellinek, Thermal degradation of isotactic and syndiotactic poly(methyl methacrylate), J. Phys. Chem. 70 (1966) 3672–3680.
[28] N. Grassie, The Chemistry of High Polymer Degradation Processes, Butterworths Scientific Publications, London, 1956.
[29] Y. Tsuboi, S. Sakashita, K. Hatanaka, H. Fukumura, H. Masuhara, Photothermal ablation of polystyrene film by 248 nm excimer laser irradiation: a mechanistic study by time-resolved measurements, Laser Chem. 16 (1996) 167–177.
[30] I.C. McNeill, L.P. Razumovskii, V.M. Goldberg, G.E. Zaikov, The thermooxidative degradation of polystyrene, Polym. Degrad. Stab. 45 (1994) 47–55.
[31] T.M. Kruse, O.S. Woo, H.W. Wong, S.S. Khan, L.J. Broadbelt, Mechanistic modeling of polymer degradation: a comprehensive study of polystyrene, Macromolecules 35 (2002) 7830–7844.
[32] B. Ranby, J.F. Rabek, Photodegradation, Photo-oxidation and Photostabilization of Polymers, Wiley, London, 1975.
[33] A. Marongiu, T. Faravelli, E. Ranzi, Detailed kinetic modeling of the thermal degradation of vinyl polymers, J. Anal. Appl. Pyrolysis 78 (2007) 343–362.
[34] T.C.K. Yang, S.S.Y. Lin, T.H. Chuang, Kinetic analysis of the thermal oxidation of metallocene cyclic olefin copolymer (mCOC)/TiO_2 composites by FTIR microscopy and thermogravimetry (TG), Polym. Degrad. Stab. 78 (2002) 525–532.